Simulation and Inference in Limit Order Books

Choon Kiat Lee

Contents

1 Introduction **2**

2 Theory **3**

2.1 Modelling . . . 3

2.1.1 Basic State Space Model . . . 3

2.1.2 Proposed State-Space Model . . . 3

2.1.3 Choice of Lévy process . . . 4

2.1.4 Solution for the proposed model . . . 4

2.1.5 Formulation of the Inference Problem in Discrete Time . . . 5

2.2 Notes on the tail approximations for alpha stable distribution . . . 5

2.3 Inference . . . 7

2.3.1 Generic Bootstrap Particle Filter . . . 7

2.3.2 Drift-Corrected Bootstrap Particle Filter . . . 7

2.3.3 Generic Rao-Blackwellised Particle Filter (RBPF) . . . 7

2.3.4 Dense Sampling Rao-Blackwellised Particle Filter (RBPF) . . . 12

2.3.5 Adaptive Sampling Rao-Blackwellised Particle Filter (RBPF) . . . 13

3 Experimental Design **17**

3.1 Simulated Data . . . 17

3.2 Performance Metrics . . . 18

3.2.1 Statistical Metrics . . . 18

3.2.2 Actual Trading Performance Metrics . . . 18

3.3 Hyperparameter selection . . . 19

3.4 Trading Algorithm . . . 19

4 Experimental Results and Discussion **19**

4.1 Comparison of inference algorithms 19
4.1.1 Drift Corrected Particle Filter 20
4.2 Rao-Blackwellised Particle Filter 23
4.3 Parameter Estimation 27
4.4 Computational Costs 27
4.5 Exploration of High Frequency Financial Timeseries 27
4.6 Trading Simulations 29

5 Discussion **29**
5.1 Efficiency 29
5.2 Timescales 29
5.3 Computational Costs 29

6 Conclusion **29**

1 Introduction

Systematic trading of financial securities is a growing field, with just over half of the trading volume in S&P 500 options attributed to high frequency algorithmic trading.

In this project, we aim to develop a *momentum*-based trading strategy. *Momentum*-based trading strategies aim to identify an ongoing price trend and then take a market position in order to benefit from its continuation. We aim to do this by developing a model for the price dynamics of the traded commodity, then use bayesian filtering techniques to track the underlying trends in the price.

The underlying dynamics of financial asset values are not clear, despite extensive study of the behaviour of asset prices. Thus, the first part of our project focuses on building a model of the underlying asset price dynamics. Since our momentum-based trading strategy relies on its ability to determine a trend to follow, we focus on developing a model which can model time-varying trends in price.

The second part of our project focuses on applying Bayesian filtering techniques for performing state inference given a state space model of price dynamics obtained in the previous part. For inference, we have explored both the use of a simple bootstrap particle filter as well as a more sophisticated Rao-Blackwellised particle filter based on a Scale Mixture of Normals (SMiN) representation of our proposed model. We have also performed parameter estimation, and have considered both maximum likelihood estimates of the mean reversion coefficient as well as fully bayesian approaches utilising state augmentation.

Lastly, we will apply our inference techniques to a real dataset of recent EURUSD exchange rates. We apply a basic trading strategy to our model, and show that it has the potential to generate excess returns in the market.

2 Theory

2.1 Modelling

2.1.1 Basic State Space Model

We build upon the model proposed by Christensen et al. [**christensen2012forecasting**] (Equation 1). In the original Christensen model, the state of the traded commodity is modelled by 2 components: "value" x_1 and "trend" x_2. These components correspond to the the price and return of the traded commodity respectively.

Insert Picture Here

Trend changes can cause difficulty for momentum strategies. This model attempts to address this issue by allowing for a finite number of discrete jumps in the trend process. This allows for modelling of sharp changes of sentiment in the market, and allow our filtered predictions to reflect these changes of sentiment more quickly than models that simply smooth the price series.

$$\begin{bmatrix} dx_{1,t} \\ dx_{2,t} \end{bmatrix} = \underbrace{\begin{bmatrix} 0 & 1 \\ 0 & \theta \end{bmatrix} \begin{bmatrix} x_{1,t} \\ x_{2,t} \end{bmatrix} dt}_{\text{Mean Reverting Returns}} + \underbrace{\begin{bmatrix} 0 \\ \sigma \end{bmatrix} dW_t}_{\text{Brownian Motion}} + \underbrace{\begin{bmatrix} 0 \\ 1 \end{bmatrix} dJ_t}_{\text{Finite-activity Gauss-Poisson jump}} \tag{1}$$

2.1.2 Proposed State-Space Model

Statistical testing has found that infinite-activity jumps (rather than finite-activity jumps) are present in high frequency stock returns [**ait2011testing**]. This might be due to significant price movements triggering stop-loss orders that prompt further trading, leading to a self-exciting series of high frequency small jumps [**osler2005stop**].

Thus, we propose modelling a tradable commodity's price using Lévy-type processes with infinite jump activity as given by Equation 2 below.

$$\begin{bmatrix} dx_{1,t} \\ dx_{2,t} \end{bmatrix} = \underbrace{\begin{bmatrix} 0 & 1 \\ 0 & \theta \end{bmatrix} \begin{bmatrix} x_{1,t} \\ x_{2,t} \end{bmatrix} dt}_{\text{Mean Reverting Returns}} + \underbrace{\begin{bmatrix} 0 \\ 1 \end{bmatrix} dL_t}_{\text{Infinite-activity Lévy process}} \tag{2}$$

We then observe the price process corrupted in gaussian noise:

$$y_t = x_{1,t} + \sigma_{obs}\eta_t, \text{ where } \eta_t \sim \mathcal{N}(0,1) \tag{3}$$

2.1.3 Choice of Lévy process

We choose use an α-stable Lévy process to capture the characteristics of the noise terms of the basic state space model provided in Equation 1 – namely the Brownian motion term and the jump term. An α-stable Lévy process has both a continuous gaussian component and an infinite-activity jump process component, which allows us to capture the noise characteristics proposed in Equation 1 in a concise manner. This also allows us to leverage existing literature developed for α-stable Lévy proceses to tackle the inference problem.

The family of α-stable distributions forms a rich class of distributions which allow for asymmetry and heavy tails. We define a real-valued random variable X to follow an stable distribution $S_\alpha(\sigma, \beta, \mu)$ if and only if its characteristic function is given by:

$$\mathbb{E}[e^{itX}] = \begin{cases} \exp\left(-\sigma^\alpha |t|^\alpha [1 - i\beta \operatorname{sign}(t) \tan(\frac{\alpha\pi}{2})] + i\mu t\right) & \alpha \neq 1 \\ \exp\left(-\sigma^\alpha |t| [1 + i\beta \frac{2}{\pi} \operatorname{sign}(t) \ln t] + i\mu t\right) & \alpha \neq 1 \end{cases} \tag{4}$$

We can then define the scalar α-stable process L_t that we will use as the driving Lévy process in our state-space model as a process which has:

- $L_0 = 0$
- Independent α-stable increments: $L_t - L_s \sim S_\alpha((t-s)^{1/\alpha}, \beta, 0), t > s$

For $1 \leq \alpha < 2$, this is a pure jump plus gaussian drift process as desired.

2.1.4 Solution for the proposed model

We consider a one-dimensional version of our proposed model which only considers the returns component (x_2).

$$dx_{2,t} = \theta x_{2,t} dt + \sigma dL_t \tag{5}$$

For the scalar case, this can be solved using results based on [**samoradnitsky2017stable**] to give a tractable state transition density:

$$f(x_{2,t}|x_{2,s}) \sim S_\alpha(\sigma_{t-s}, \beta, \exp(\theta(t-s)x_{2,s}), \qquad \sigma_{\delta t} = \left(\sigma \frac{\exp(\alpha\theta\delta t) - 1}{\alpha\theta}\right)^{1/\alpha} \tag{6}$$

2.1.5 Formulation of the Inference Problem in Discrete Time

Using the solution to the one-dimensional version of the proposed model in Equation 6, we can formulate our original continuous-time state space model as a discrete-time state space model where the parameters of the discrete-time state matrices $\mathbf{A}(\delta t)$ and $\mathbf{b}(\delta t)$ vary according to the continuous time solution and the gap to the previous time step, δt.

For brevity, we will assume in all subsequent equations that $\mathbf{A}$ and $\mathbf{b}$ are implicitly dependent on δt, and will drop this explicit dependence.

This approach allows us to use established techniques used for discrete time inference.

$$\begin{aligned} \mathbf{x}_t &= \mathbf{A}(\delta t).\mathbf{x_{t-1}} + \mathbf{b}(\delta t).L_t \\ y_t &= \mathbf{C}.\mathbf{x}_t + \mathbf{d}.\eta_t \\ \text{where} \qquad \delta_t &= T_t - T_{t-1} \\ l_t &\sim S_{\alpha/2}(1,1,0) \text{ and } \eta_t \sim \mathcal{N}(0,1) \end{aligned} \tag{7}$$

2.2 Notes on the tail approximations for alpha stable distribution

We take a brief segue to provide some theory into the tail approximation to the α-stable distribution that will be useful in the later sections.

When $\alpha < 2$, the tails of the α-stable distribution are are asymptotically equivalent to a Pareto law. More precisely, if λ is a standardized α-stable variable $\lambda \sim S_\alpha(\sigma, \beta, \mu)$ with $0 < \alpha < 2$, $\sigma = 1$, $\mu = 0$ then as $\lambda \to \infty$ ([**samoradnitsky2017stable**]):

$$\lim_{x\to\infty} P(\lambda > x) = C_\alpha(1+\beta)x^{-\alpha} \tag{8}$$

where:

$$C_\alpha = \left(2\int_0^\infty x^{-\alpha}\sin x dx\right)^{-1} = \frac{1}{\pi}\Gamma(\alpha)\sin(\frac{\alpha\pi}{2})$$

We can then differentiate Equation 8 to obtain the pdf of the tail approximation:

$$\begin{aligned}\lim_{x \to \infty} S_\alpha(\lambda = x | \sigma = 1, \beta, \mu = 0) &= f_{pareto}(\lambda = x | \alpha, \beta) \\ &= \alpha C_\alpha (1 + \beta) x^{-\alpha - 1}\end{aligned} \tag{9}$$

Numerical accuracy of the tail approximation

We first define a metric for the absolute relative error in the tail approximation:

$$\epsilon_{rel}(x) = \left| \frac{S_\alpha(\lambda = x|1, \beta, 0) - f_{pareto}(\lambda = x|\alpha, \beta)}{S_\alpha(\lambda = x|1, \beta, 0)} \right| \tag{10}$$

We can then investigate the numerical accuracy of the tail approximation for $\beta = 1$ and $\alpha < 1$ using Figure 1. As expected, we note that the relative error in the tail approximation decreases monotically.

Note that for $\alpha < 1$, there is no clear dependence on the value of α and the rate of convergence of the α-stable distribution to the paretian tail approximation.

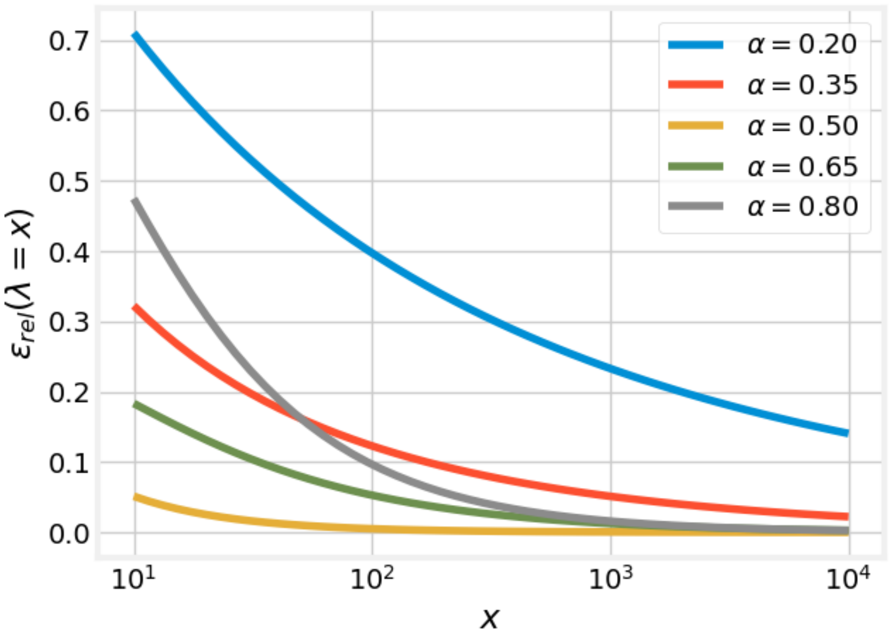

Figure 1: Relative error in the tail approximation $\epsilon_{rel}(x)$ for $\beta = 1$ and $\alpha < 1$

Sampling from the paretian tail

Using the paretian tail approximation to the α-stable distribution , we note that up to a certain scale parameter$(\alpha(1+\beta)C_\alpha)$, sampling from a left-truncated α-stable distribution can be approximated by sampling from a left-truncated pareto distribution.

For a left-truncated pareto distribution $f_{pareto}(x|\alpha,\beta)$ lower bounded by $x \geq L$, we the corresponding PDF $f_{bounded\ pareto}(x|\alpha,\beta,L)$ is given by Equation 11:

$$f_{bounded\ pareto}(x|\alpha,\beta,L) = \alpha L^\alpha \left(\frac{x}{\alpha(1+\beta)C_\alpha}\right)^{-\alpha-1} \tag{11}$$

We can then sample from this left-truncated pareto distribution easily using the inverse transform method.

$$x = \alpha(1+\beta)C_\alpha \left(\frac{1-U}{L^\alpha}\right)^{-\frac{1}{\alpha}} \qquad \text{where: } U \sim \text{Unif}(0,1) \tag{12}$$

Following Equation 12, x will be left-truncated pareto distributed according to $f_{bounded\ pareto}(x|\alpha,\beta,L)$

2.3 Inference

2.3.1 Generic Bootstrap Particle Filter

2.3.2 Drift-Corrected Bootstrap Particle Filter

To combat the problem of drift, we incorporate a discrete integration approximation to the price process (x_1) into our state space model (Equation 13). This allows us to use numerical integration to obtain an estimate of the current inferred value of the price process at every time step that can then be used to correct for price drift in the system. This drift-corrected state space model (Equation 13) forms the basis of all further explorations.

$$\underbrace{\begin{bmatrix} x_{1,t+\delta t} \\ x_{2,t+\delta_t} \end{bmatrix}}_{\mathbf{S_{t+\delta t}}} = \underbrace{\begin{bmatrix} 1 & \delta t \\ 0 & e^{\theta\delta t} \end{bmatrix}}_{\mathbf{A}} \underbrace{\begin{bmatrix} x_{1,t} \\ x_{2,t} \end{bmatrix}}_{\mathbf{S_t}} + \underbrace{\begin{bmatrix} 0 \\ 1 \end{bmatrix}}_{\mathbf{b}} L_t, \qquad L_t \sim S_\alpha(\sigma_{\delta t},\beta,0) \tag{13}$$

2.3.3 Generic Rao-Blackwellised Particle Filter (RBPF)

Scale Mixture Of Normals (SMiN) Representation

In foreign exchange markets such as the EUR/USD, market moves are widely regarded to be symmetric in nature [**tankov2003financial**]. This motivates the selection of the parameter

$\beta = 0$. Instead of considering the general α-stable process, we can instead restrict ourselves to a more analytically tractable sub-class, the a Symmetric α-stable (SαS) process instead.

For $\beta = 0$, we have a convenient Scale Mixture of Normals (SMiN) representation based off the product property of α-stable distributions: If X and Y are independent random variables with $\lambda_t \sim S_{\alpha/2}(1,1,0)$ and $\eta_t \sim S_2(1,0,0) = \mathcal{N}(0,1)$, then $\lambda_t\eta_t \sim S_\alpha(1,0,0)$.

We can then convert the discretised state space model specified in Equation 13 into SMiN form as specified in Equation 14 below.

$$\underbrace{\begin{bmatrix} x_{1,t+\delta t} \\ x_{2,t+\delta_t} \end{bmatrix}}_{\mathbf{x_{t+\delta t}}} = \underbrace{\begin{bmatrix} 1 & \delta t \\ 0 & e^{\theta\delta t} \end{bmatrix}}_{\mathbf{A}} \underbrace{\begin{bmatrix} x_{1,t} \\ x_{2,t} \end{bmatrix}}_{\mathbf{x_t}} + \underbrace{\begin{bmatrix} 0 \\ \sigma_{\delta t} \end{bmatrix}}_{\mathbf{b}} \sqrt{\lambda_{t+\delta t}}\eta_{t+\delta t}; \qquad \eta_{t+\delta t} \sim \mathcal{N}(0,1),\ \lambda_{t+\delta t} \sim S_{\alpha/2}(1,1,0) \tag{14}$$

This means that conditional upon us observing $\lambda_{t+\delta t}$, $\mathbf{x}_{t+\delta t}$ is gaussian, making inference much more tractable. We exploit this fact by designing a Rao-Blackwellised Particle Filter to sample $\lambda_{t+\delta t}$ by using a simple particle filter, and propogating the states using a Kalman Filter conditioned upon the sampled $\lambda_{t+\delta t}$ of the particle.

We take a short detour to properly formulate the inference problem using the SMiN representation here. In the inference problem, we are seeking to infer the state variables $\mathbf{x}_{t+\delta t}$ given the observations $y_{t+\delta t}$. Changing indexes using $k = t + \delta t, k - 1 = t$, to reflect the discretised nature of the problem, we assume model dynamics as follows:

$$\begin{aligned} \mathbf{x}_k &= \mathbf{A}\mathbf{x}_{k-1} + \mathbf{b}\sqrt{\lambda_k}\eta_k \\ y_k &= \mathbf{C}\mathbf{x}_k + d\epsilon_k \\ \lambda_k &\sim S_{\alpha/2}(1,1,0) \\ \eta_k, \epsilon_k &\sim \mathcal{N}(0,1) \end{aligned} \tag{15}$$

It will also be useful to use the following expression for y_k:

$$\begin{aligned} y_k &= \mathbf{CAx}_{k-1} + \underbrace{\begin{bmatrix} \mathbf{Cb}\sqrt{\lambda_k} & d \end{bmatrix}}_{\mathbf{e}_k} \underbrace{\begin{bmatrix} \eta_k \\ \epsilon_k \end{bmatrix}}_{\mathbf{n_k}} \qquad (16) \\ \mathbf{n}_k &\sim \mathcal{N}(\mathbf{0}, \mathbf{I}) \\ \lambda_k &\sim S_{\alpha/2}(1,1,0) \end{aligned}$$

This transforms our state equation form into a (nearly?) α-stable sub-gaussian form. (This is NOT in α-stable sub-gaussian form, see: $<$ α-stable sub-gaussian definition $>$ for reference)

Generic Rao-Blackwellised Particle Filter (RBPF)

For Rao-Blackwellised Particle Filtering, we partition the state vector into gaussian and non-gaussian components. We can then use standard Kalman Filtering to obtain optimal estimates for the gaussian state components, after obtaining estimates for the non-gaussian state components.

At each time step k, the Rao-Blackwellised Particle Filter produces for each time step k a set of weighted samples $\left\{w_k^{(i)}, \lambda_k^{(i)}, \mu_k^{(i)}, \Sigma_k^{(i)} : i = 1, ..., N\right\}$ according to:

1. Draw new latent variables $\lambda_t^{(i)}$ for each particle in $i = 1, ..., N$ from the corresponding importance distribution:

$$\lambda_k^{(i)} \sim \pi(\lambda_k | \lambda_{0:k-1}^{(i)}, y_{1:k}) \qquad (17)$$

For the generic RBPF, we choose the importance distribution:

$$\pi(\lambda_k | \lambda_{0:k-1}^{(i)}, y_{1:k}) = p(\lambda_k | \lambda_{0:k-1}^{(i)}) = S_{\alpha/2}(\lambda_k | 1, 1, 0) \qquad (18)$$

2. Calculate new weights as follows:

$$w_k^{(i)} \propto w_{k-1}^{(i)} \frac{p(y_k | \lambda_{0:k}^{(i)}, y_{1:k-1}) p(\lambda_k^{(i)} | \lambda_{k-1}^{(i)})}{\pi(\lambda_k^{(i)} | s_{0:k-1}^{(i)}, y_{1:k})} \qquad (19)$$

Here, the likelihood term $p(y_k | u_{0:k}^{(i)}, y_{1:k-1})$ is obtained using the predictive error decomposition from the Kalman Filter:

Kalman Filtering Prediction Step:

$$
\begin{aligned}
p(\mathbf{x}_{0:k}|\lambda_{0:k}^{(i)}, y_{1:k-1}) &= \mathcal{N}(\mathbf{x}_k|\mu_k^{-(i)}, \Sigma_k^{-(i)}) \qquad (20)\\
\text{where:} \qquad \mu_k^{-(i)} &= \mathbf{A}\mu_{k-1}^{(i)}\\
\Sigma_k^{-(i)} &= \mathbf{A}\Sigma_{k-1}^{-(i)}\mathbf{A}^T + \mathbf{b}^T\mathbf{b}\lambda_k^{(i)}
\end{aligned}
$$

Predictive Error Decomposition:

$$
\begin{aligned}
p(y_k|\lambda_{0:k}^{(i)}, y_{1:k-1}) &= \int p(y_k|\lambda_{0:k}^{(i)}, \mathbf{x}_{0:k})p(\mathbf{x}_{0:k}|\lambda_{0:k}^{(i)}, y_{1:k-1})d\mathbf{x}_{0:k}\\
&= \mathcal{N}(y_k|\mathbf{C}\mu_k^{-(i)}, \mathbf{C}\Sigma_k^{-(i)}\mathbf{C}^T + d^2) \qquad (21)
\end{aligned}
$$

3. Perform Kalman Filter updates for each of the particles conditional on the drawn latent variables $\lambda_k^{(i)}$.

$$
\begin{aligned}
p(\mathbf{x}_{0:k}|\lambda_{0:k}^{(i)}, y_{1:k}) &= \mathcal{N}(\mathbf{x}_k|\mu_k, \Sigma_k) \qquad (22)\\
\text{where:} \qquad \mathbf{v}_k^{(i)} &= y_k - \mathbf{C}\mu_k^{(i)}\\
\mathbf{S}_k^{(i)} &= \mathbf{C}\Sigma_k^{-(i)}\mathbf{C}^T + d^2\\
\mathbf{K}_k^{(i)} &= \Sigma_k^{-(i)}\mathbf{C}^T\mathbf{S}_k^{-1}\\
\\
\mu_k^{(i)} &= \mu_k^{-(i)} + \mathbf{K}_k^{(i)}\mathbf{v}_k^{(i)}\\
\Sigma_k^{(i)} &= \Sigma_k^{-(i)} - \mathbf{K}_k^{(i)}\mathbf{S}_k^{(i)}[\mathbf{K}_k^{(i)}]^T
\end{aligned}
$$

4. Perform multinomial resampling to increase the number of effective particles.

Potential Problems with the RBPF

When $y_k - \mathbf{C}\mathbf{A}\mu_k^{(i)}$ is large, the RBPF is often unable to get a good importance sampling estimate for λ_k.

When $y_k - \mathbf{C}\mathbf{A}\mu_k^{(i)}$ is large, this implies that λ_k is likely to be large also. (See Figure 3, noting that $p(\lambda_k|y_k - \mathbf{C}\mathbf{A}\mu_k^{(i)}) \propto S_{\alpha/2}(\lambda_k)\mathcal{N}(y_k - \mathbf{C}\mathbf{A}\mu_k^{(i)}|\lambda_k))$. As a large λ_k lies in the low probability right tail of the particle proposal distribution given by Equation 18, very few particles $\lambda_k^{(i)}$ are generated from the particle proposal distribution which are close to the actual λ_k.

This problem is exacerbated by the fact that the α parameter of the proposal distribution is half of the original α. This causes the tails of the proposal distribution is to decay very slowly, increasing the number of particles needed to give a good importance sampling estimate.

This results in sample impoverishment, whereby there are only a few effective particles with non-negligible weights, which causes the performance of the RBPF to be slightly worse for very low numbers of particles.

One method of quantifying sample impoverishment in a particle filter (whilst adjusting for number of particles) is by measuring the entropy of the particle filter weights given in Equation 23.

$$H(w) = \sum_{i=1}^{N} w_i \log(w_i) \qquad \text{where: } \sum_{i=1}^{N} w_i = 1 \tag{23}$$

In order to compare the entropy of the particle weights across different number of particles, we instead use a normalised entropy measure given in Equation 24.This normalised entropy measures the change in entropy between a set of weights with uniform distribution (an ideal "optimized" set of weights) and a set of weights with a non-uniform distribution, and is scaled to be independent of the number of particles, as well as the base used in calculating the entropy.

$$H_n(w) = \frac{1}{\log_b(N)} \sum_{i=1}^{N} w_i \log_b(w_i) \qquad \text{where: } \sum_{i=1}^{N} w_i = 1 \tag{24}$$

We demonstrate the problem of sample impoverishment by simulating a single time step of the particle filter, for varying values of $y_k - \mathbf{CA}\mu_k^{(i)}$. Fixing $\mu_k^{(i)}$, $\Sigma_k^{(i)}$ whilst varying y_k and N, we simulate one time step of the RBPF update step described above and present the normalised entropy of the particle filter weights obtained in Figure 2. We see that the normalised entropy of the particle filter weights drops rapidly for large $y_k - \mathbf{CA}\mu_k^{(i)}$, and that the as N increases, the normalised entropy of the particle filter weights is more resistant to sample impoverishment at large values of $y_k - \mathbf{CA}\mu_k^{(i)}$ as expected.

Dense Sampling

Adaptive Sampling

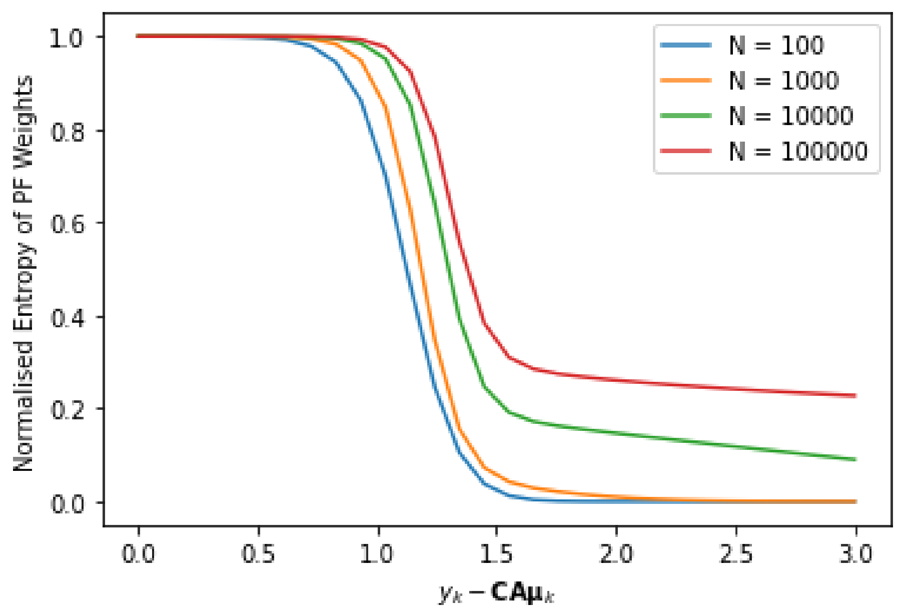

Figure 2: Change in normalised entropy of PF weights as $y_k - \mathbf{CA}\mu_k^{(i)}$ and N are varied

2.3.4 Dense Sampling Rao-Blackwellised Particle Filter (RBPF)

We note that the cause of the problem of sample impoverishment is due to the low number of particles being drawn from the tails of the proposal distribution, leading to low numbers of particles with effective weights when $y_k - \mathbf{CA}\mu_k^{(i)}$ is large

Thus, one method of reducing sample impoverishment in the particle filter would be to simply generate a larger number of particles from the tails of the proposal distribution. In order to preserve the required proposal distribution, we need to then scale the weights of the extra particles generated from the tails appropriately.

This leads to the following algorithm for sampling from the proposal distribution given in Equation 18:

- Define the hyperparameters ϵ_λ and m. In this example, we select $\epsilon_\lambda = 1 \times 10^{-1}$ and $m = 3$.
- Calculate the number of extra particles (N_{extra}) to draw from the right tail using:

$$threshold = \frac{f_{pareto}(\lambda_k|\alpha/2, 1) - S_{\alpha/2}(\lambda_k|1, 1, 0)}{S_{\alpha/2}(\lambda_k|1, 1, 0)} \tag{25}$$

$$N_{extra} = P(\lambda > threshold) \times Nm \tag{26}$$

- Draw N_{extra} particles from the right tail:

$$\lambda_k^{(i)} \sim f_{bounded\ pareto}(\lambda_k|\alpha = \alpha/2, \beta = 1, L = threshold) \qquad i = 1...N_{extra} \tag{27}$$

- Draw $N - N_{extra}$ particles from the truncated alpha stable distribution using a simple rejection sampler:
  - Draw $\lambda_k^{(i)} \sim S_{\alpha/2}(\lambda_k|1, 1, 0)$
  - Accept if $\lambda_k^{(i)} < threshold$
- Alter the weights of the particles drawn from the tails:

$$w_i = \frac{1}{m} w_i \qquad \text{for: } i \in [1, N_{extra}]$$

2.3.5 Adaptive Sampling Rao-Blackwellised Particle Filter (RBPF)

One way of attempting to improve the performance of the RBPF is to form a better importance sampling distribution. In this section, we seek to form a better importance sampling distribution for $\pi(\lambda_t|y_{1:t}, \lambda_{0:t-1})$.

For optimality, we want $\pi(\lambda_t|y_{1:t}\lambda_{0:t-1}^{(i)}) \approx p(\lambda_t|y_{1:t}, \lambda_{0:t-1}^{(i)})$.

It is hard to formulate an analytical form for this density directly. To get around this, we can instead form the analytical joint distribution for $p(y_t, \lambda_t|y_{1:t-1}, \lambda_{0:t-1}^{(i)})$. The complete derivation is given in the appendix, with the key steps highlighted below.

We first augment the probability density given above with $x_{0:t-1}$. This allows us to use results from the previously-performed Kalman Filter step.

$$\begin{aligned}
& p(y_t.\lambda_t, x_{0:t-1}|y_{1:t-1}, \lambda_{0:t-1}^{(i)}) \\
\propto\ & p(y_t|y_{1:t-1}, \lambda_{0:t}^{(i)}, x_{0:t-1}) p(x_{0:t-1}|y_{1:t-1}, \lambda_{0:t}^{(i)}) p(\lambda_t^{(i)}|\lambda_{0:t-1}^{(i)}) \\
\approx\ & p(y_t|y_{1:t-1}, \lambda_{0:t}^{(i)}, x_{0:t-1}) p(x_{0:t-1}|y_{1:t-1}, \lambda_{0:t-1}^{(i)}) p(\lambda_t|\lambda_{0:t-1}) \\
=\ & \mathcal{N}(y_t|\mathbf{CA}\mathbf{x}_{t-1}, \mathbf{e}\mathbf{e}^T) \mathcal{N}(\mathbf{x}_{0:t-1}|\mu_k^{(i)}, \mathbf{\Sigma}_k^{(i)}) S_{\alpha/2}(1, 1, 0) \\
=\ & \mathcal{N}\left(\begin{bmatrix} y_t \\ \mathbf{x}_{t-1} \end{bmatrix} \middle| \begin{bmatrix} \mathbf{CA}\mu_{k-1}^{(i)} \\ \mu_{k-1}^{(i)} \end{bmatrix}, \begin{bmatrix} \mathbf{e}\mathbf{e}^T + (\mathbf{CA})\mathbf{\Sigma}_k^{(i)}(\mathbf{CA})^T & \mathbf{CA}\mathbf{\Sigma}_k^{(i)} \\ \mathbf{\Sigma}_k^{(i)}(\mathbf{CA})^T & \mathbf{\Sigma}_k^{(i)} \end{bmatrix} \right) S_{\alpha/2}(1, 1, 0)
\end{aligned}$$

We can then obtain the required density $p(y_t, \lambda_t^{(i)}|y_{1:t-1}, \lambda_{0:t-1})$ by marginalising out $x_{0:t-1}$:

$$
\begin{aligned}
p(y_k, \lambda_k|y_{1:k-1}, \lambda_{0:k-1}^{(i)}) &= \int p(y_k, \lambda_k, x_{0:k-1}|y_{1:k-1}, \lambda_{0:k-1}^{(i)})dx_{0:k-1} \\
&= \mathcal{N}(y_k|\mathbf{CA}\mu_k^{(i)}, (\mathbf{Cb})(\mathbf{Cb})^T\lambda_k + d^2 + (\mathbf{CA})\mathbf{\Sigma}_k^{(i)}(\mathbf{CA})^T)S_{\alpha/2}(\lambda_t|1,1,0) \\
&= \mathcal{N}(y_k|\mathbf{CA}\mu_k^{(i)}, \sigma_\lambda\lambda_k + \mu_\lambda)S_{\alpha/2}(\lambda_t|1,1,0) \qquad (28)
\end{aligned}
$$

where:

$$
\begin{aligned}
\sigma_\lambda &= (\mathbf{Cb})(\mathbf{Cb})^T \\
\mu_\lambda &= d^2 + (\mathbf{CA})\mathbf{\Sigma}_k^{(i)}(\mathbf{CA})^T
\end{aligned}
$$

By fixing the value of y_k in Equation 28, we can obtain the desired distribution $p(\lambda_k|y_{1:k}, \lambda_{0:k-1})$.

This formulation of the joint distribution also gives us an alternative interpretation for the sampling density $p(\lambda_t|y_{1:t}, \lambda_{0:t-1})$.

We can reinterpret this as finding the posterior density of λ_k given the observations $y_t - \mathbf{CA}\mu_k$. The prior on λ_k is the α-stable proposal distribution $S_{\alpha/2}(\lambda_k|1,1,0)$ while the likelihood is the unknown variance of a normal distribution ($\mathcal{N}(y_t|\mathbf{CA}\mu_k, \sigma_\lambda\lambda_t + \mu_\lambda)$).

Rejection Sampling

In general, there is no closed form expression for this distribution. However, we can utilise the fact that we can draw samples from the prior distribution easily using the Chamber-Mallow-Stuck method [**chambers1976method**]. This can be used as a suitable proposal function for rejection sampling.

We adapt the methods of [**godsill1999bayesian**] to draw samples from this distribution.

The target distribution for the rejection sampling scheme is given by:

$$
\begin{aligned}
f(y_t, \lambda_t|y_{1:t-1}, \lambda_{0:t-1}^{(i)}) &= \mathcal{N}(y_t|\mathbf{CA}\mu_k^{(i)}, \sigma_\lambda\lambda_t + \mu_\lambda)S_{\alpha/2}(\lambda_t|1,1,0) \\
&= \mathcal{N}(y_t - \mathbf{CA}\mu_k^{(i)}|, \sigma_\lambda\lambda_t + \mu_\lambda)S_{\alpha/2}(\lambda_t|1,1,0)
\end{aligned}
$$

Using a proposal distribution $g(\lambda_t|y_{1:t}, \lambda_{0:t-1}) = S_{\alpha/2}(1,1,0)$, we can use the likelihood as a valid rejection function as it is bounded from the above:

$$\begin{aligned}\mathcal{N}(y_t - \mathbf{C}\mathbf{A}\mu_k^{(i)}|0, \sigma_\lambda\lambda_t + \mu_\lambda) &\leq \frac{f(y_t, \lambda_t|y_{1:t-1}, \lambda_{0:t-1})}{g(y_t, \lambda_t|y_{1:t-1}, \lambda_{0:t-1})} \\ &= M\end{aligned}$$

$$M = \begin{cases} \frac{1}{\sqrt{2\pi(y_t - \mathbf{C}\mathbf{A}\mu_k^{(i)})^2}} \exp(-0.5) & (y_t - \mathbf{C}\mathbf{A}\mu_k^{(i)})^2 \geq \mu_\lambda \\ \frac{1}{\sqrt{2\pi d^2}} \exp\left(-\frac{(y_t - \mathbf{C}\mathbf{A}\mu_k^{(i)})^2}{2d^2}\right) & (y_t - \mathbf{C}\mathbf{A}\mu_k^{(i)})^2 \leq \mu_\lambda \end{cases} \tag{29}$$

This gives a suitable rejection sampler as:

1. Draw $\lambda_k \sim S_{\alpha_2}(1, 1, 0)$
2. Draw $u \sim U(0, M)$
3. If $u \geq \mathcal{N}\left(y_t - \mathbf{C}\mathbf{A}\mu_k^{(i)}|0, \sigma_\lambda\lambda_k + \mu_\lambda\right)$, reject λ_t and go to Step (1)

Improvements on the rejection sampler:

The rejection sampler suffers from poor acceptance rates when $y_k - \mathbf{C}\mathbf{A}\mu_k^{(i)}$ is very large. Most of the samples generated by the prior fall into the left tail of the likelihood, and have extremely low probabilities of being accepted (Figure 3).

Due to the additional observation noise term (d), we are unable to use the Inverse Gamma approximation to the full posterior as detailed in [**godsill1999bayesian**]. Instead, we attempt to improve the sampling efficiency by truncating the left tail of the likelihood distribution.

Due to the intractability of calculating the Cumulative Distribution Function (CDF) of the likelihood analytically, we left-truncate the likelihood where it is smaller than a chosen epsilon. In this project, this small epsilon was chosen to be $\epsilon_{trunc} = 1 \times 10^{-9}$. Further checks are also performed to ensure that this truncation only occurs well into the right tail of the prior.

This allows us to generate samples from a left-truncated form of the α-stable prior instead of the full prior. These generated samples are much more likely to be in the high probability regions of the likelihood, thus improving our sampling efficiency greatly.

We sample from the left truncated α-stable distribution by applying a paretian tail approximation to the α-stable distribution , then sampling from the paretian tail approximation using Equation 12.

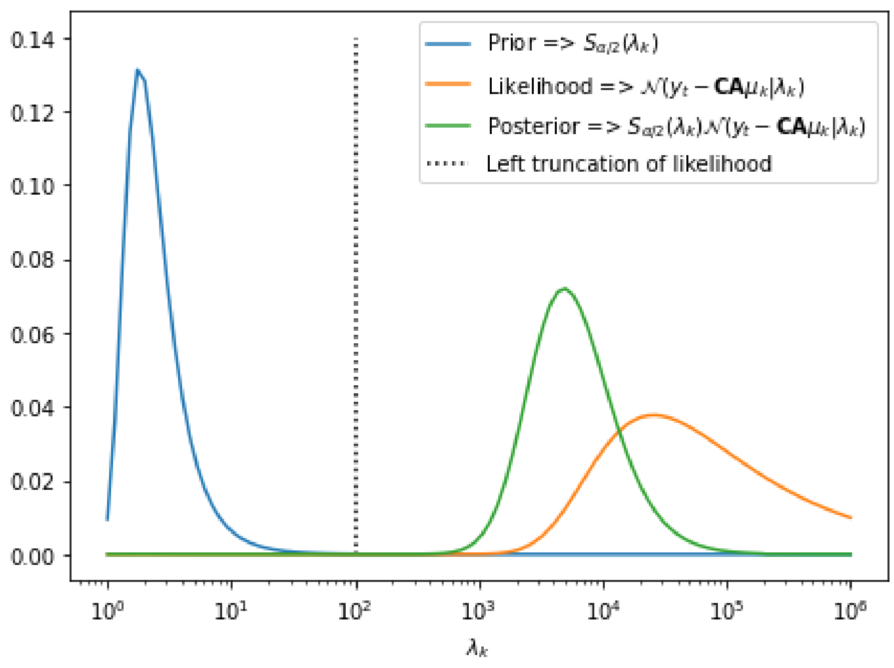

Figure 3: Illustration of the poor acceptance rate regime of prior/likelihood interaction

This improved rejection sampler can be described as:

1. Define hyperparameter ϵ_{trunc}
2. Calculate 95th percentile of the prior ($\lambda_{0.95}$) where: $\int_0^{\lambda_{0.95}} S_{\alpha/2}(\lambda_k|1,1,0) = 0.95$
3. Draw proposals $\lambda_k^{(i)}$
   - Calculate a possible truncation value $\lambda_{k,trunc}$ where $\mathcal{N}(y_k - \mathbf{CA}\mu_k^{(i)}|\lambda_{k,trunc}) = \epsilon_{trunc}$.
   - If this truncation value also lies in the right tail of the prior (i.e. $\lambda_{k,trunc} > \lambda_{0.95}$) then sample particle from the paretian tail approximation

$$\lambda_k^{(i)} \sim f_{bounded\ pareto}(x|\alpha/2, \beta = 1, \lambda_{k,trunc})$$

   - Otherwise, sample particle from the original prior:

$$\lambda_k^{(i)} \sim S_{\alpha/2}(1, 1, 0)$$

4. Draw $u \sim U(0, M)$

5. If $u \geq \mathcal{N}\left(y_k - \mathbf{CA}\mu_k^{(i)}|0, \sigma_\lambda \lambda_k + \mu_\lambda\right)$, reject $\lambda_k^{(i)}$ and go to Step (3)

3 Experimental Design

3.1 Simulated Data

In order to objectively evaluate the performance of our inference algorithms, we simulate the price and returns of a tradable commodity using the 2 dimensional discrete time state space model described in Equation 13. This provides us with the ground truth state that we can use to compare with the inferred state estimates from our particle filter.

This also allows us to check that the model has the appropriate characteristics that we are looking for.

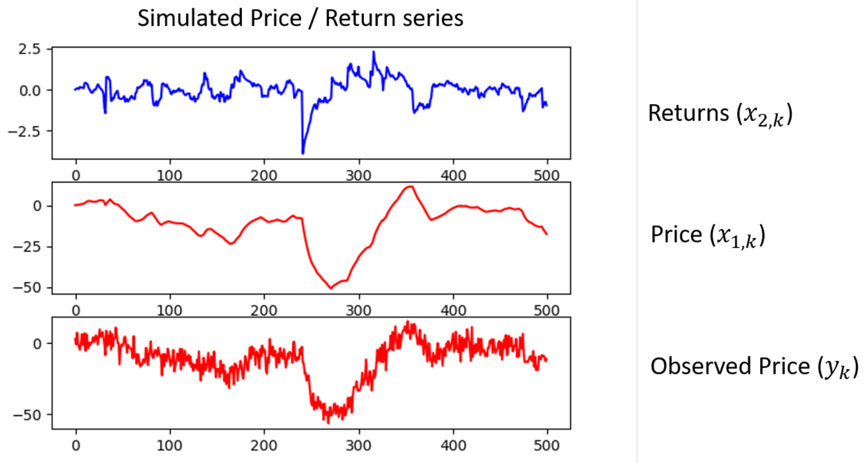

Figure 4: Simulation Results for 500 iterations

Figure 4 shows a simulated price(x_1) / returns(x_2) series, together with the observed price series corrupted by gaussian noise(y).

We note that the returns series has the desired jump activity, together with a gaussian drift back to zero mean. The gaussian drift back to zero mean allows for a predictable trend to be captured in the price process, while the jump activity allows for sharp changes in the trend.

This shows that the state-space model described in Equation 13 is able to capture both a predictable trend in asset prices, as well as sharp changes in these trends, both extremely useful for a momentum-based strategy.

3.2 Performance Metrics

3.2.1 Statistical Metrics

Mean Square Error

The mean square error (MSE) is used to compare forecasts with the real future observed state. This allows us to assess the predictive power of the inference algorithms that we are testing.

The mean square error is defined over all time points K as:

$$MSE = \mathbb{E}(e^2) = \frac{1}{K}\sum_{i=1}^{K}(y_i - \hat{y}_i)^2 \tag{30}$$

3.2.2 Actual Trading Performance Metrics

As we are interested in optimising the inference algorithms described in this paper for practical use, we want to select a performance metric that more closely reflects the actual results achieved if the filtering model is used as the backend for a real trading system.

Binary Prediction Error

One rudimentary trading algorithm that could be employed to transform the filtered state into actual trading signals simply invests a set amount of money if the predicted return is positive, and shorts the same amount if the predicted return is negative.

This simple trading algorithm will generate profits if the sign of the predicted returns matches that the sign of the actual returns.

Thus, one metric that we could use to measure the performance of the trading system looks to see how many times the sign of the predicted returns matches the sign of the actual returns (Binary Prediction Error).

This provides a more realistic measure of the profitability of this particular trading system. A binary prediction error $BPE < 0.5$ indicates that the filtered signal is predicting correct trade decisions more often than not.

We define the binary prediction error formally as:

$$
\begin{aligned}
& & BPE = \frac{1}{N}\sum_{i=1}^{N} b_i & \\
& where: & b_i = \begin{cases} 0 & \text{sign}(y_i) = \text{sign}(\hat{y}_i) \\ 1 & \text{otherwise} \end{cases} & \qquad (31)
\end{aligned}
$$

Sharpe Ratio

Instead of the simple trading algorithm detailed above, we might instead want to use more sophisticated ways of converting the filtered signal into an actual trading signal.

We can quantify the trading profitability of this actual trading signal by running the trading algorithm and obtaining the actual backtested realised returns. Using these realised profits, we can use the *sharpe ratio* of the actual realised profits to objectively evaluate the performance of the algorithm.

The sharpe ratio measures the average return earned per unit of risk(volatility) undertaken, and is defined by:

$$
\text{Sharpe Ratio} = \frac{\text{Mean of Portfolio Returns}}{\text{Standard Deviation of Portfolio Returns}} \qquad (32)
$$

Because the sharpe ratio is defined in units of risk, it can help to explain if the returns obtained are due to a profitable trading signal or simply as a result of taking on too much risk. The greater the sharpe ratio, the better its risk-adjusted performance, hence indicating that the trading signal is more profitable.

3.3 Hyperparameter selection

3.4 Trading Algorithm

4 Experimental Results and Discussion

4.1 Comparison of inference algorithms

We have implemented a total of 5 methods for conducting inference on the continuous time state space model described by Equation 2.

1. A generic one-dimensional bootstrap particle filter (PF) which inferred only the returns (x_2) state.

2. A drift-corrected bootstrap particle filter which infers both price (x_1) and returns (x_2) states simultaneously.
3. A Rao-Blackwellized Particle Filter (RBPF) for the case of a symmetrical α-stable distribution ($\beta = 0$)
4. Dense Sampling improvement for the RBPF to reduce sample impoverishment
5. Adaptive Sampling improvement for the RBPF to create a fully adapted RBPF

In this section, we will compare and discuss the results obtained by the 5 inference algorithms. Unless explicitly stated, simulated data (with the simulation process described in Secion X) has been used to obtain the results in this section. This provides us with both ground truth data for the states, as well as the actual parameters used, allowing us to test the effectiveness of the inference algorithms without the complications of parameter inference.

As a brief comparison of all the 5 inference algorithms, Figure 5 shows the performance of all 5 inference algorithms using a large number of particles ($N = 10000$).

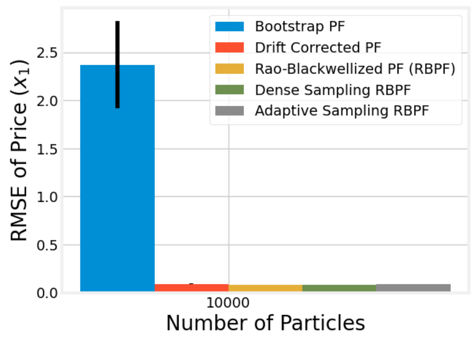

(a) Root Mean Square Error (RMSE) of the price(x_1) process

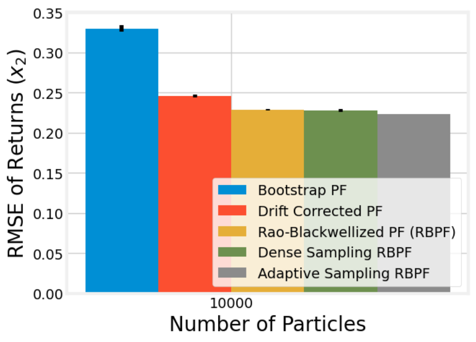

(b) Root Mean Square Error (RMSE) of the returns(x_2) process

Figure 5: Comparison of all inference algorithms, $N = 10000$ particles

We can conceptually divide the 2 inference algorithms into 2 classes: generic particle filtering based inference and rao-blackwellized particle filtering based inference. We will compare and discuss these 2 classes of inference algorithms separately in the next 2 subsections.

4.1.1 Drift Corrected Particle Filter

We first compare the results of with the generic one dimensional bootstrap particle filter of Section X and the drift-corrected particle filter described in Equation 13.

To compare the results of both particle filtering methods, we use a dataset consisting of 60 minutes of high frequency tick data for the EUR/USD currency pair from the 16th of October 2019, totalling 4196 discrete price observations.

Figure 6 gives both the observed and inferred returns and price process for the simple bootstrap particle filter. We can clearly see the effectiveness of the noise removal in the inferred returns process. However, we note that the inferred price process suffers greatly from drift. Small errors in the inference of the returns process are compounded, leading to the inferred price process deviating from the observed price.

This causes the poor inference results when the generic particle filter is used to infer the underlying price process of the simulated signal in Figure 5a.

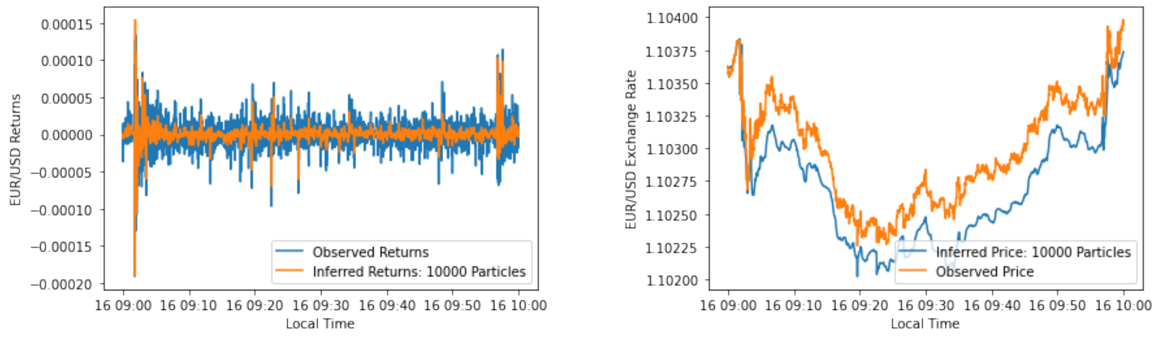

(a) Inferred Returns Process (b) Inferred Price Process

Figure 6: Simple Bootstrap Particle Filter, $N = 10000$ particles

The drift-corrected particle filter attempts to correct for price drift in the system by using numerical integration to obtain an estimate of the current inferred value of the price process at every time step.

Figure 7a gives both the observed and inferred returns and price process for the drift-corrected particle filter. We note qualitatively that the inferred returns process shows much greater noise reduction, and the inferred price process no longer suffers from price drift.

Varying N

Figure 8 shows how the performance of the 2 bootstrap particles filters vary as the number of particles, N is changed. Here, we apply between the ground truth underlying price and return states from simulated data and the inferred underlying price and return states from the particle filters. This allows us to examine how well the particle filter tracks the actual underlying state.

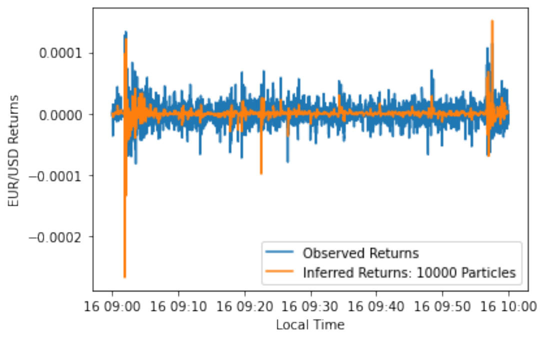

(a) Inferred Returns Process

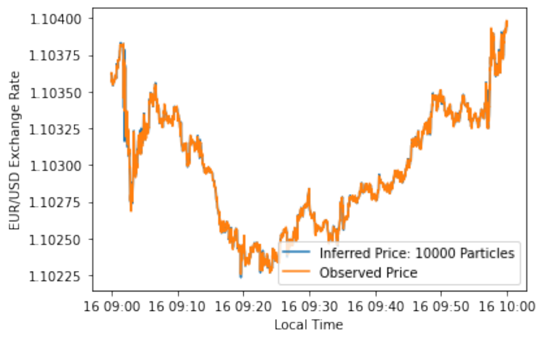

(b) Inferred Price Process

Figure 7: Drift-Corrected Particle Filter, $N = 10000$ particles

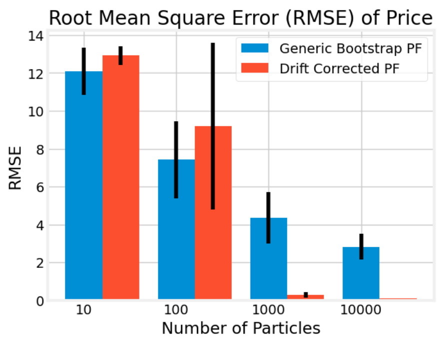

(a) RMSE of price(x_1) state

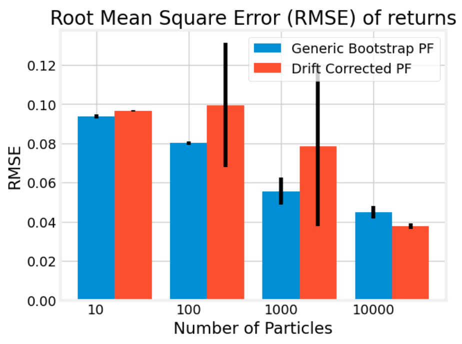

(b) RMSE of returns(x_2) state

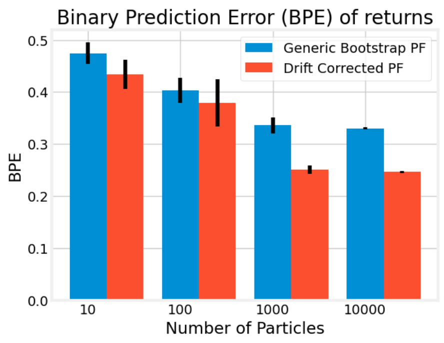

(c) BPE of returns(x_2) state

Figure 8: Comparison of inference performance between the 2 bootstrap particle filters as N varies

Both the generic bootstrap particle filter and the drift-corrected particle filter are both very sensitive to sample impoverishment in the same manner as described in **??**.

For low N and large $y_k - \mathbf{C}\mathbf{A}\mathbf{x}_{k-1}^{(i)}$, the samples of $\mathbf{x}_k$ obtained from the particle filter proposal distribution are likely to have very low acceptance weights, resulting in a lack of particles with effective weights. If there are no particles with effective weights generated by the particle filter, the tracking performance of the particle filter can be severely diminished. The larger the observed price outlier ($y_k - \mathbf{C}\mathbf{A}\mathbf{x}_{k-1}^{(i)}$) and the lower the number of particles N, the greater the impact of this problem.

Thus, we expect the performance of the bootstrap particle filters to fall rapidly as the number of particles drops. Furthermore, we also expect the RMSE achieved by the bootstrap particle filters to be more variable at low numbers of particles.

We also note that the Binary Prediction Error (BPE) of the returns process is much less affected by low numbers of particles as compared to the RMSE. Optimising for BPE only requires the particle filter to predict the correct *direction* of returns, and is hence a less challenging task compared to accurately forecasting the underlying return state (measured by RMSE). This is encouraging, as it implies that the actual trading performance of the particle filters is likely to be less affected by the random initialisations of the particles filter, and hence is likely to be more robust to outliers in the data. For $N = 1000$ and $N = 10000$, we also note that the BPE (0.25) is much lower than a BPE based solely on change (0.5), indicating that the bootstrap particle filters are frequently able to correctly predict the direction of the underlying return state.

4.2 Rao-Blackwellised Particle Filter

Comparison of inference performance

Figure 9 shows how the performance of the 2 bootstrap particles filters vary as the number of particles, N is changed.

Firstly, we note that the performance of the 3 RBPF-based particle filters is in general better than the bootstrap particle filters across all performance metrics. This suggests that the ability of the RBPF-based particle filters to marginalise out the gaussian components of the hidden state is very useful in improving the inference performance of the particle filter.

Secondly, we note that in general, the performance of the dense sampling RBPF and the adaptive sampling RBPF is slightly better than that of the generic RBPF, suggesting that the dense sampling and adaptive sampling improvements are both useful in improving the inference performance of the generic RBPF. Figures 9a and 9b indicate that the performance of the generic RBPF degrades significantly as the number of particles (N) used drops, likely due to sample impoverishment. However, the dense sampling RBPF and adaptive sampling

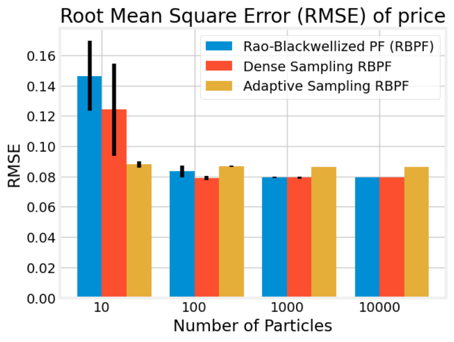

(a) RMSE of price(x_1) state

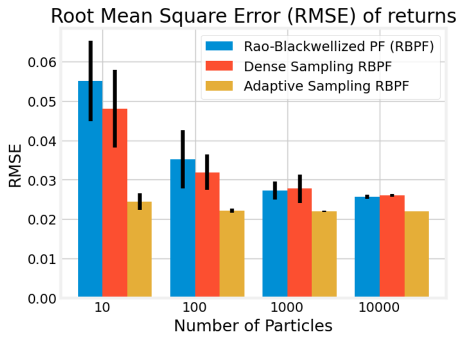

(b) RMSE of returns(x_2) state

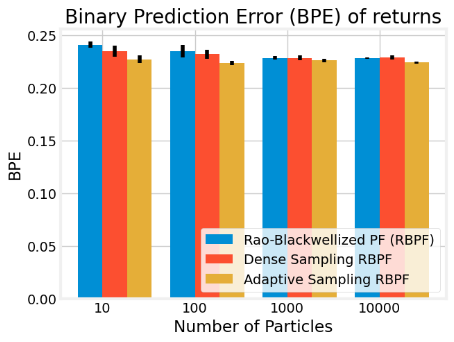

(c) BPE of returns(x_2) state

Figure 9: Comparison of inference performance between the 3 RBPF-based particle filters as N varies

RBPF are both more resistant to this degradation in performance, indicating that they are likely less affected by sample impoverishment.

In particular, the adaptive sampling RBPF is extremely resistant to the degradation in performance as the number of particles drops, with good inference performance even with as low as 10 particles.

Dense Sampling RBPF

We now examine the reduction in sample impoverishment due to the dense sampling improvement described in **??**.

Similarly to **??**, we demonstrate the problem of sample impoverishment by simulating a single time step of the particle filter, for varying values of $y_k - \mathbf{CA}\mu_k^{(i)}$. Fixing $\mu_k^{(i)}$, $\Sigma_k^{(i)}$ whilst varying y_k and N, we simulate one time step of the RBPF update step described above and present the normalised entropy of the RBPF particle weights with and without the dense sampling improvement in Figure 2.

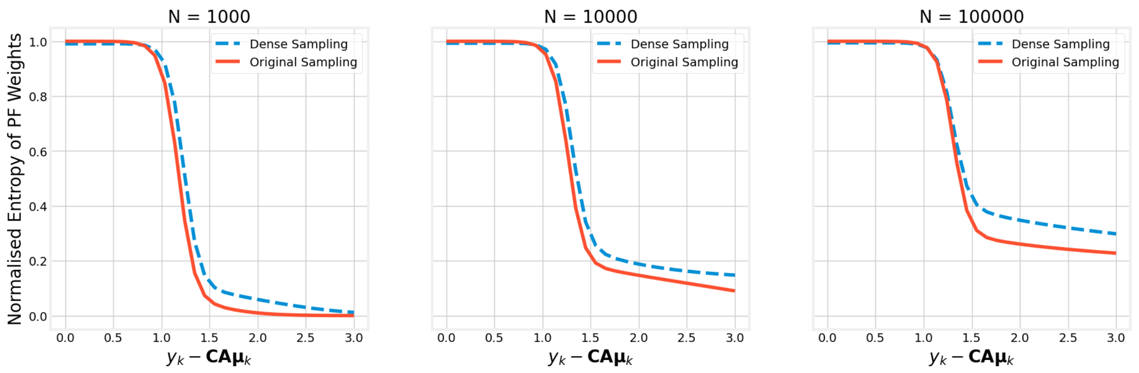

Figure 10: Improvement in normalised entropy of RBPF particle weights using dense sampling with hyperparameters: ($\epsilon_\lambda = 0.1$, $m = 2$)

We can see from Figure 2 that the dense sampling improvement causes the normalised entropy of the RBPF particle weights to increase for larger price outliers $y_k - \mathbf{CA}\mu_k^{(i)}$. A higher normalised entropy indicates that the weights of the RBPF particles are more evenly distributed and hence that there are a larger number of particles with effective weights under the dense sampling improvement.

Adaptive Sampling RBPF

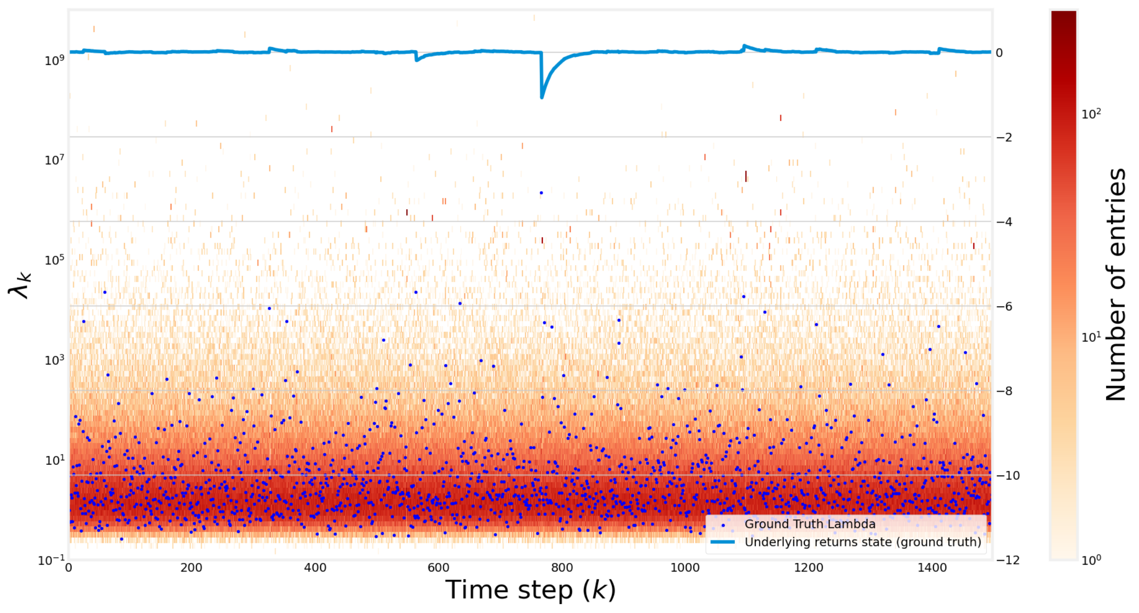

Figure 11: Distribution of samples $\lambda_k^{(i)}$ from the Generic RBPF

Figure 11 shows the distribution of samples $\lambda_k^{(i)}$ from the Adaptive Sampling RBPF as well as the ground truth λ_k used to generate the simulation data. Figure 12 shows a similar figure for the generic RBPF *after* the resampling step.

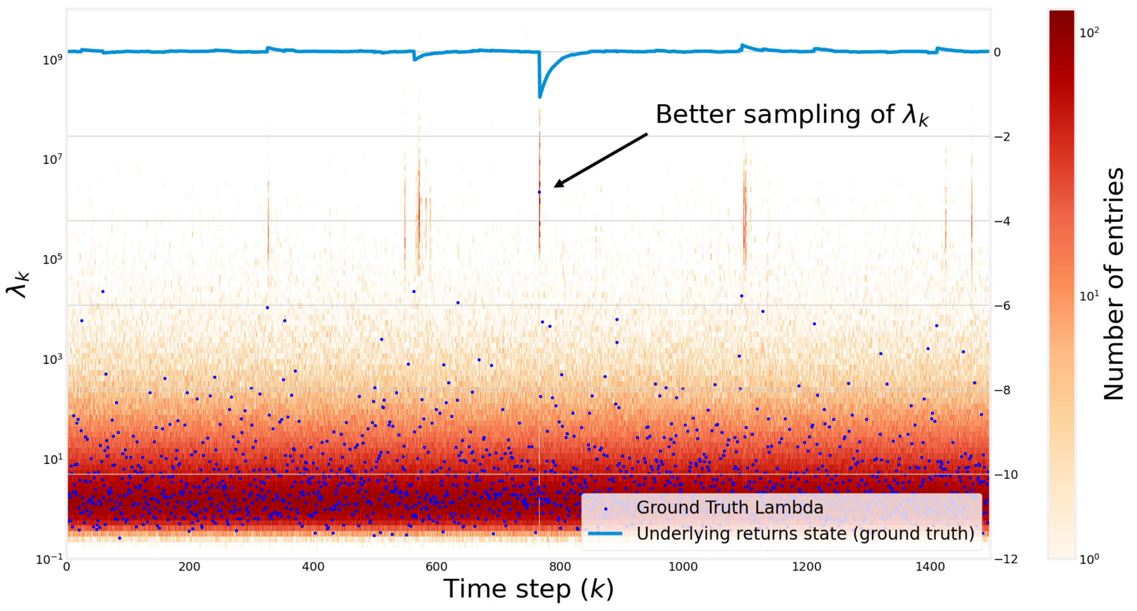

Figure 12: Distribution of samples $\lambda_k^{(i)}$ from the Adaptive Sampling RBPF

Comparing Figures 11 and 12, we can see qualitatively that the distribution of samples from the Adaptive Sampling RBPF is distributed more closely around the ground truth λ_k, resulting in a many more effective samples being generated using the Adaptive Sampling RBPF compared to the generic RBPF.

Note the extremely challenging nature of forming a good importance sampling estimate of the posterior $p(\lambda_k|y_k, \mu_{k-1}, \Sigma_{k-1})$ using only samples from the prior as λ_k ranges over 7 orders of magnitude (10^{-1} to 10^7) in this example. This makes it very difficult to form a good discrete importance sampling estimate, which would require a huge amount of particles to cover the entire possible range of λ_k (which theoretically has infinite support). With the adaptive sampling improvement, we are able to use the information from the current observation to sample directly from the approximate posterior, which increases the sampling efficiency of the particle filter greatly.

We next investigate how few particles we can use with the new adaptive sampling particle filter before performance degrades unacceptably. Figure 13 shows how the RMSE of the inferred underlying returns process changes for very low values of N. Interestingly, we note that the adaptive sampling RBPF is still capable of good inference performance even with extremely low $N = 4$, unlike the generic RBPF, which suffers from degradation of inference performance when using a low number of particles.

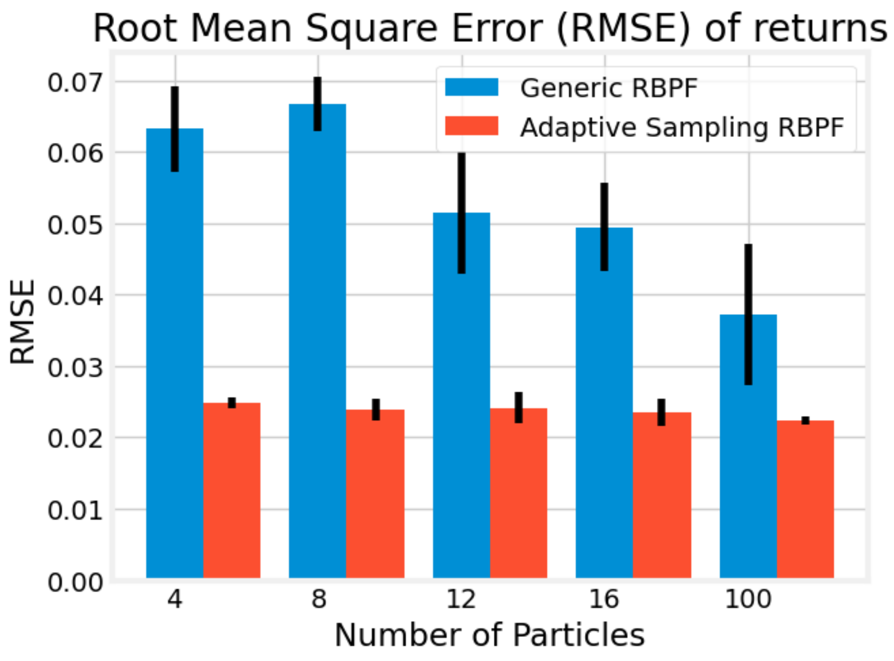

Figure 13: Performance of the RBPF-based particle filters for very low N

4.3 Parameter Estimation

4.4 Computational Costs

4.5 Exploration of High Frequency Financial Timeseries

Origin

The focus of these experiments will be on foreign exchange data.

The main dataset used for testing has been obtained through the Swiss online foreign exchange bank, Dukascopy. We focus mainly on the highly liquid EUR/USD currency pair, which has a high trading frequency.

Due to the global nature of the foreign exchange market

We use 2 different types of foreign exchange data for testing: tick level data and daily price level data.

Tick level data is a high frequency stream-like list of transactions, with new events arriving over 100 times per second. For each transaction, we receive the transaction price together with the next closest buy (bid) and sell (ask) prices to the transaction price.

Daily price level data consists of the market price at each the time of market close.

We will mainly work with the high frequency tick level data in our project, exploring the limits of how

However, we will use the daily price level data to compare the results of our exploration.

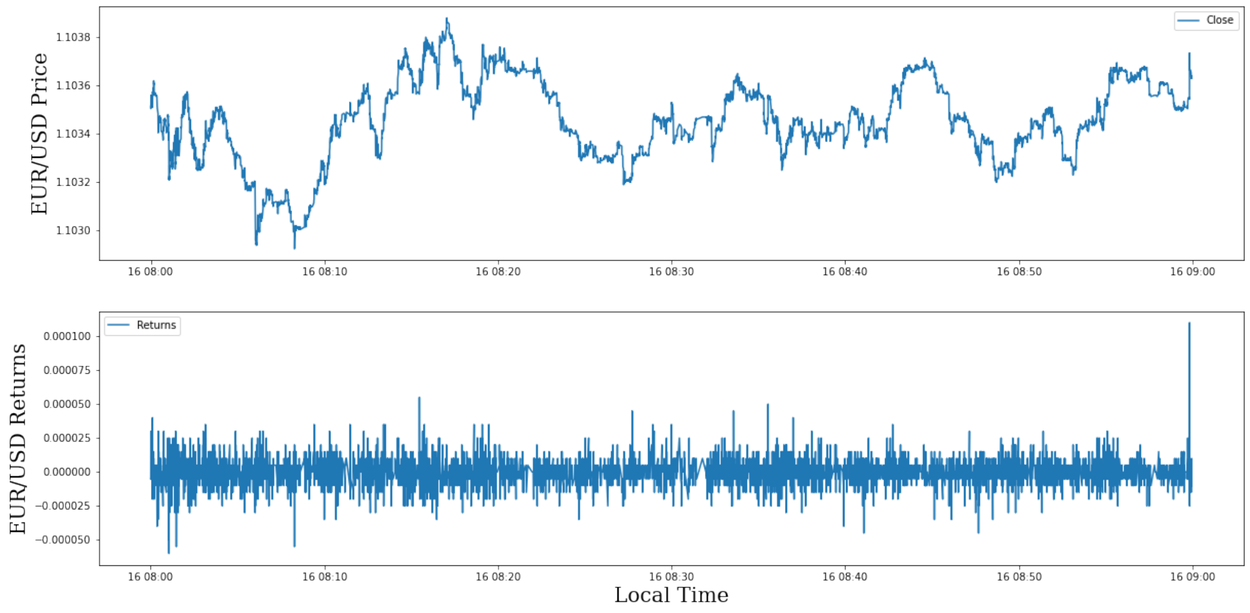

(a) Example of EUR / USD Tick Level Data, 1600 - 1700 on 10/02/2019

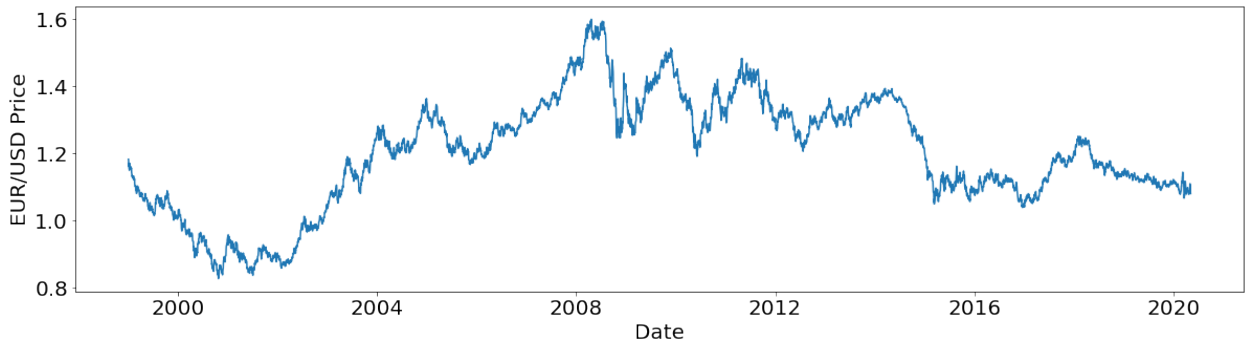

(b) Example of EUR / USD Daily Close Data, 1999 - 2020

Quantisation

The high frequency tick data that we obtain is often *quantized*, and consists of only a few price levels. This is typical, as exchanges do not allow arbitrary prices to be transacted. In this case, the minimum price change possible is $5x10^-6EUR/USD$.

This is a violation of one of the core assumptions of the stochastic modelling: that the price levels are continuous. As the minimum return ($5x10^-6$) is small compared to the standard deviation of the returns, we ignore this problem in the project. However, we note that this could be a problem in extremely high frequency trading, where the price does not fluctuate much, hence causing the minimum return to be significant compared to the standard deviation of returns.

4.6 Trading Simulations

5 Discussion

5.1 Efficiency

5.2 Timescales

5.3 Computational Costs

6 Conclusion

List of Figures

1 Relative error in the tail approximation $\epsilon_{rel}(x)$ for $\beta = 1$ and $\alpha < 1$ 6

2 Change in normalised entropy of PF weights as $y_k - \mathbf{CA}\mu_k^{(i)}$ and N are varied 12

3 Illustration of the poor acceptance rate regime of prior/likelihood interaction 16

4 Simulation Results for 500 iterations 17

5 Comparison of all inference algorithms, $N = 10000$ particles 20

6 Simple Bootstrap Particle Filter, $N = 10000$ particles 21

7 Drift-Corrected Particle Filter, $N = 10000$ particles 22

8 Comparison of inference performance between the 2 bootstrap particle filters as N varies 22

9 Comparison of inference performance between the 3 RBPF-based particle filters as N varies 24

10 Improvement in normalised entropy of RBPF particle weights using dense sampling with hyperparameters: ($\epsilon_\lambda = 0.1$, $m = 2$) 25

11 Distribution of samples $\lambda_k^{(i)}$ from the Generic RBPF 25

12 Distribution of samples $\lambda_k^{(i)}$ from the Adaptive Sampling RBPF 26

13 Performance of the RBPF-based particle filters for very low N 27

List of Tables